Engineering Fracture Mechanics 110 (2013) 38–51

Contents lists available at ScienceDirect

Engineering Fracture Mechanics

journal homepage: www.elsevier.com/locate/engfracmech

# Fracture energy of the concrete–FRP interface in strengthened beams

Mithila Achintha [a,*], Chris Burgoyne [b]

[a] Faculty of Engineering and the Environment, University of Southampton, Southampton SO17 1BJ, UK
[b] Department of Engineering, University of Cambridge, Trumpington Street, Cambridge CB2 1PZ, UK

ARTICLE INFO

*Article history:*
Received 22 April 2012
Received in revised form 16 July 2013
Accepted 17 July 2013
Available online 11 August 2013

*Keywords:*
Debonding
Fracture mechanics
Interface
Mixed-mode
Strengthened beams

ABSTRACT

To determine the load at which FRPs debond from concrete beams using global-energy-balance-based fracture mechanics concepts, the single most important parameter is the fracture energy of the concrete–FRP interface, which is easy to define but difficult to determine. Debonding propagates in the narrow zone of concrete, between the FRP and the (tension) steel reinforcement bars in the beam, and the presence of nearby steel bars prevents the fracture process zone, which in concrete is normally extensive, from developing fully. The paper presents a detailed discussion of the mechanism of the FRP debonding, and shows that the initiation of debonding can be regarded as a Mode I (tensile) fracture in concrete, despite being loaded primarily in shear. It is shown that the incorporation of this fracture energy in the debonding model developed by the authors, details of which are presented elsewhere, gives predictions that match the test results reported in the literature.


## 1. Introduction

This paper addresses fracture energy of the concrete–FRP interface that is important in the analysis of the debonding of FRP plates from concrete beams, and forms part of a much larger study [1–3]. The authors have previously developed a fracture mechanics model to analyse FRP debonding; the model has been validated against many experiments carried out by others [3]. The earlier work of validating the FRP debonding model required knowledge of the fracture energy of concrete; this is not a parameter that is normally measured when performing experiments. The current paper explains why particular values for the fracture energy of concrete were used in the earlier work of validating the FRP debonding model against experimental results.

Premature FRP debonding hampers efficient use of externally bonded FRP plates in flexural strengthening of concrete beams, and uncertainty about the governing mechanisms means that there is no reliable theory that can be applied by designers. Debonding initiates from the propagation of a dominant crack in the vicinity of the concrete–FRP interface, and hence fracture-mechanics-based finite element (FE) approaches have often been used in the literature to determine failure load [4]. These analyses were often based on the pioneering theories of Hutchinson and Suo [5], which were intended for the analysis of interface debonding in thin-layered elastic materials. However, in contrast to materials like glass, it is generally assumed that the fracture process zone (FPZ) in concrete is large, typically over 300 mm long with a width of several times the aggregate size [6]. As a result, the concrete–FRP interface cannot be modelled using the concepts of linear elastic fracture mechanics (LEFM).

* Corresponding author. Tel.: +44 (0)7500197739.
*E-mail address:* Mithila.Achintha@soton.ac.uk (M. Achintha).

0013-7944/$ - see front matter © 2013 Elsevier Ltd. All rights reserved.
http://dx.doi.org/10.1016/j.engfracmech.2013.07.016

**Nomenclature**

| | |
|---|---|
| $C$ | concrete cover thickness |
| $d_a$ | maximum size of the aggregates used in the concrete mix |
| $F_p$ | force in the FRP |
| $f'_c$, $f_t$ | compressive and tensile strength of concrete respectively |
| $G$ | energy release rate |
| $G_C$ | fracture energy of concrete |
| $G_{CI}$, $G_{CII}$ | Modes I and II fracture energy of concrete respectively |
| $G_F$, $G_{F\_int}$ | fracture energy and interface fracture energy respectively |
| $h$ | depth of the beam |
| $l_d$ | length of the debonding crack |
| $L_0$ | distance from the nearest beam support to the FRP plate curtailment location |
| $L_{0\_e}$ | distance from the nearest beam support to the effective plate end location |
| $P_f$ | failure load of test beams |
| $w$ | width of the separation between the two surfaces of a crack/fracture process zone |
| $w_c$ | critical crack opening in Mode I fracture |
| $\sigma$ | normal stress |

Nonlinear FE models, such as the J-integral method that would be needed to simulate FRP debonding, require far more detail of the interface properties (such as the distribution of voids in the interface between the adhesive and the concrete, and knowledge of the aggregate distribution) than will ever be available to the designers. It should be noted that, despite FE analyses being capable of providing accurate solutions for complex structural mechanics problems such as fracture in metals, the technique is not proven as a reliable tool for analyses of concrete structures [7]. The unreliable and unknowable material descriptions hamper accurate FE modelling of concrete structures; the results from a detailed FE model largely depend on the assumptions made by the analyst on the distribution of voids in the interface between the adhesive and the concrete, and knowledge of the aggregate distribution. It should also be considered the fact that concrete can crack and it can also creep differentially; modelling these effects are difficult. Furthermore, since concrete cracks at very low tensile strains ($\sim$0.0002), even a small error in the analysis sometimes can seriously distort the solutions. In particular, although magnitudes of the minor stress components are smaller than the main stress their effects may cause cracks in concrete. Thus, the material properties of concrete should refer to the response under a generalised 3-D state of stress. However, the triaxial data of the material properties are difficult to obtain and often shows a great deal of scatter even in closely monitored experimental programmes [8].

In a conventional FE analysis, the crack path must be known *a priori*; a crack follows the path of least resistance around or through the aggregate, but reliable estimates for relative fracture resistances of aggregates and the interface between aggregate/cement-paste cannot be made. Alternatively, the use of smeared-crack based FE models avoids the need to model discrete cracks, but the analyses fail to model debonding, which is triggered by the propagation of a dominant single crack. There have been a number of recent hybrid continuous-discontinuous FE approaches and extended FE methods (XFEM), which allow moving from diffuse damage patterns to discrete (dominant) crack propagation and also the propagation of various discontinuities. Similarly, specially defined cohesive elements, which do not represent any physical material, but describe the cohesive forces that may occur when material elements are being pulled apart, can be also used to model the FPZ of concrete [8]. Despite these FE modelling approaches have been used to model fracture problems in various applications such as interface debonding in thin layered materials, the methods so far have not been used to model concrete fracture. Typically, elements significantly smaller than the size of aggregate (size of aggregate >10 mm) are needed in FE simulations to obtain consistent results, but at this length scale, concrete does not behave as a homogeneous material. As a further complication in the analysis of FRP debonding, the effect of the steel bars present in the FPZ is difficult to model (Fig. 1). It may be possible to incorporate this effect by imposing a boundary condition in the form of a known strain constraint but no acceptable method exists in the literature.

A high stress may cause a crack to form near the interface, but that crack will only propagate if more energy is thereby released than it takes to form the new fracture surfaces. It is thus a fracture mechanics problem so an accurate solution cannot be determined from methods based on a detailed stress analysis. In recently developed non-linear fracture mechanics models [9], the results of shear-lap tests were used to derive the fracture parameters that govern FRP debonding. However, as is shown below, these tests do not provide accurate fracture parameters that can be used in the analysis because of the difference between the mode of fracture that takes place in strengthened beams and that in a shear-lap test. In addition, the FRP carries a very high tension force ($F_p$), acting at an eccentricity with respect to the tip of the shear/flexural crack that forms the critical interface crack. This introduces a significant tension at the crack tip causing a tensile fracture; none of the reported studies take account of this effect. As an alternative, Oehlers et al. [10] recently presented a model, based on the rigid-body rotations that take place at the dominant flexural crack that triggers debonding. This model, however, re-

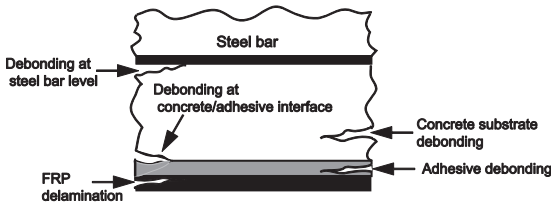


**Fig. 1.** Possible phases for the initiation of the dominant interface crack.

quires precise details of the crack locations and only considers the effect of a single flexural crack in the beam. Although a number of models have been reported, none of this provides a comprehensive tool to analyse FRP debonding.

The present authors have earlier developed a global-energy-balance-based fracture mechanics model for the analysis of FRP debonding [1–3,11]. The model obviates the need for FE analyses. The model assumes that flaws are inevitable in the interface, and predicts that debonding will occur when the energy available to drive a small extension of an existing interface crack exceeds the energy needed to form the new fracture surfaces. Two key governing parameters are compared in the model to determine debonding: the energy release rate (i.e. the energy release due to a unit extension of a crack of unit width–$G$) and the interface fracture energy (the energy required to form new fracture surfaces needed to accommodate a unit extension of a crack of unit width–$G_{F\_int}$). Manufacturers have now developed sufficiently tough adhesives that, if used correctly, failure usually takes place in the concrete just above the interface (Fig. 1). Thus, it is possible to assume that $G_{F\_int}$ is the same as the fracture energy of concrete ($G_C$). The *critical crack* – i.e. the smallest crack that can propagate rapidly under the given conditions – can be determined when $G = G_C$. Thus, for a given beam, the model can determine either the crack length that triggers failure at the design load, or the failure load of a beam with an existing crack of known length. The model predictions, based on this concept adopted in the analyses, matched well with test data reported in the literature [3].

When the fracture occurs, the beam loses some of its stiffness, so work is done by the external loads. The curvature increases in the beam, storing some of this extra work as strain energy, but some is left over to cause the crack to propagate. The $G$ during fracture extension can be determined if the energy states of the beam before and after the crack extension are known [1,2]. An accurate analysis of the energy state of a beam using its stress–strain variations over the whole span is very complex, so a simpler integration of moment–curvature ($M$–$\kappa$ was used, but even determining the curvature is complex [1]. A modified form of Branson's model [12], which determines the $M$–$\kappa$ relations and hence the energy state of a beam was developed; this analysis is presented elsewhere [1,2].

If the technique of flexural strengthening of beams is to be useful, it is necessary to know the $G_C$ of the concrete from which the beam is made. But $G_C$ is not a property that can be determined reliably, either theoretically or experimentally. To determine $G_C$ theoretically, knowledge of the stress–displacement relations in the FPZ are required, and it is more accurate to rely on experimental investigations. However, inconsistent fracture data can result from experiments since the FPZ may not develop fully in the small specimens usually used in experiments. Also, it is difficult to set up experiments to accurately simulate the interface mixed-mode stresses that trigger FRP debonding from concrete beams [2].

This paper raises a number of issues that are controversial, and go against accepted wisdom; the logic will be explained in more detail below.

- Conventional fracture analysis would fail to determine the $G_C$ in the vicinity of the interface, because the FPZ cannot develop fully due to the presence of the steel bars.
- FRP debonding from concrete beams can be regarded as a Mode I fracture in concrete, which explains why the shear-lap experiments often used in the literature do not provide results that are useful. Instead, it is necessary to use data from experiments designed to determine the tensile fracture energy. The paper shows how the fracture energies of the beams quoted in the earlier papers by the authors [3] were determined.
- The fracture energy can be regarded as independent of the length of the debonding crack, even though the FPZ cannot develop fully, because the strain conditions near the tip of the crack remain unchanged as the crack develops.
- The data provided by this analysis can be used to predict debonding loads in a range of strengthened beams that have been reported in the literature.

## 2. Mechanism of FRP debonding

The plate end, and zones where widening of flexural cracks cause interface flaws, are most susceptible to the initiation of debonding; the two modes are referred to as "plate-end" (PE) and "intermediate-crack-induced" (IC) debonding respectively [2]. PE debonding initiates at the vicinity of the FRP end and propagates towards the middle of the beam, whereas IC debonding initiates at a high-moment zone and propagates towards a low-moment zone (Fig. 2). Debonding propagates within the concrete substrate and usually the whole concrete cover separates in PE debonding whereas a thin concrete layer separates in IC debonding [4].

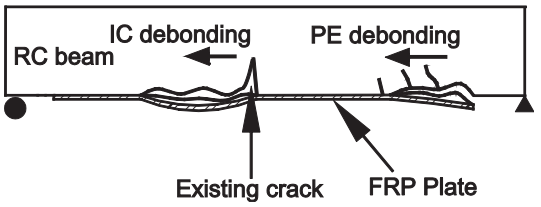


**Fig. 2.** Two modes of debonding.

### 2.1. Interfacial stress concentrations

A crack in a material can propagate either by opening (Mode I), shearing between the two crack faces (Mode II), or by a combination of both (mixed-mode). In different modes of fracture, different stress–displacement fields will develop in the vicinity of the crack, so the fracture energy depends on which fracture mode occurs. Although cracks in brittle, isotropic, homogeneous solids propagate by maintaining pure Mode I condition at the crack tip, the stress field that triggers debonding at an interface can be very complex [5]. Various forms of stress concentrations develop due to the different fracture toughnesses of the two joining materials and also due to the number of geometric constraints present in the vicinity [5].

#### 2.1.1. Plate-end (PE) debonding

If the FRP plate is curtailed at a considerable distance away from the beam support, a dominant shear crack can be formed in the concrete beam near the plate end (Fig. 3a). There are two mechanisms that may cause the crack to propagate towards the beam along a direction about 45° to the interface (Fig. 3a). The FRP force acts at an eccentricity with respect to the tip of this shear crack, where it induces significant tension (Fig. 3a). The crack will propagate by opening of the crack tip in the direction perpendicular to that of the maximum principal tensile stress (MPTS). The relative vertical displacements between the two crack faces of the original shear crack can also contribute to the propagation of the crack towards the beam.

Various other mechanisms can also introduce additional interfacial stress concentrations. The concrete beam is very stiff by comparison with the FRP, so the beam remains effectively straight, while the eccentricity between the tension in the FRP and the concrete surface tends to peels away the FRP from the beam. Moreover, the axial strain of the FRP is zero at its ends, but since the FRP is curtailed at a nonzero moment location, the adjacent surface of concrete has a nonzero axial strain. The stress gain in the FRP at its end is very rapid and is associated with a development of significant interfacial shear stresses. These interfacial stress concentrations cause the propagation of the original shear crack, however because of the presence of the steel bars, PE debonding usually takes place at the level of the steel.

#### 2.1.2. Intermediate-crack-induced (IC) debonding

The relative sliding between the two faces of a flexural crack in a high moment zone of the beam forms interface flaws, and these movements of the crack faces will also introduce the peeling force that is required to trigger debonding (Fig. 3b). In addition, the transfer of tensile stresses from the concrete to the FRP at the crack location introduces high interfacial shear stresses. If the stress concentrations that develop at the interface crack exceed the critical state, debonding takes place towards a low moment zone of the beam (Fig. 2). Note that, since the principal stress would be at about 45° to the interface, it is expected that the crack would move into the beam. However, this will not happen since a high $F_p$ acts eccentrically to the crack tip, taking the fracture back down towards the interface (Fig. 3a). Thus, a thin layer of concrete separates here, in comparison to that during PE debonding.

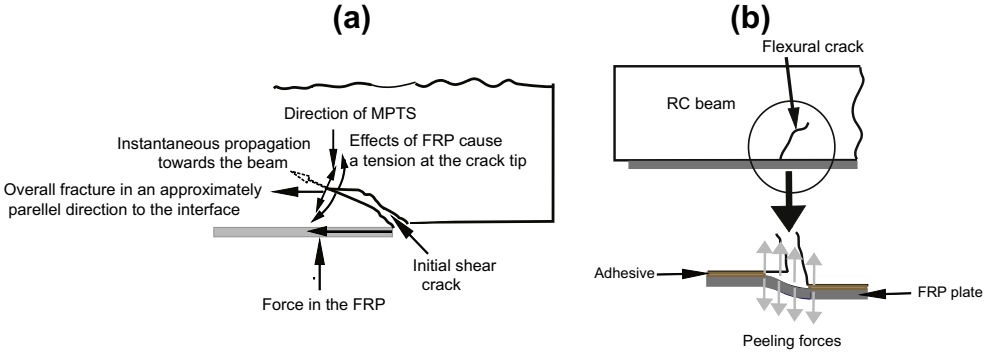


**Fig. 3.** (a) Effect of the FRP causes a significant tension at the tip of the shear crack during PE debonding. (b) Relative sliding between the two faces of flexural cracks causes interface flaws that trigger IC debonding.

A complex stress field that develops in the vicinity of a critical interface crack triggers debonding. A knowledge of fracture energy of concrete against mixed-mode loading is therefore needed to determine the loads at which debonding occurs, although it will be contended below that the Mode I effects dominate the propagation of debonding. Note that it is virtually impossible to accurately determine these crack-tip stress fields and therefore any method that purports to compare predicted detailed stresses with interface strength is almost guaranteed not to provide a reliable solution.

## 3. Fracture energy of concrete under mixed-mode loading

A crack under mixed-mode loading can experience either kinking or straight-ahead propagation, depending on the relative fracture resistances associated with the competing possible directions of advance [5]. The mixed-mode fracture energy ($G_{CI/II}$) thus depends on the respective fracture energies of pure primary modes (i.e. $G_{CI}$ and $G_{CII}$ respectively) and also on the magnitude of the component of each primary mode of fracture involved during a unit total extension of the crack (Eq. (1)) [5]. The relative contributions of each primary mode (i.e. the mode mixity–$\psi$) is defined as the ratio of the components of Mode II to Mode I. $G_{CI/II}$ usually increases with the increase of $\psi$ since $G_{CII}$ is often higher than $G_{CI}$. In linear elastic fracture mechanics the mode mixity ($\psi$) is defined as:

$$\psi = \tan^{-1}(K_{II}/K_I) \tag{1}$$

where $K_I$ and $K_{II}$ are stress intensity factors of pure Mode I and Mode II respectively.

### 3.1. Mechanism and fracture energy of Mode I crack

Under uniaxial tension, when the applied stress at the tip of an existing crack reaches the tensile strength ($f_t$), the crack starts to open in the direction perpendicular to that of the stress. A new portion of the crack is formed in front of the crack tip, and thus, the crack starts to propagate by opening (i.e. Mode I crack) (Fig. 4a). However, until the tip of the original crack (Point A in Fig. 4a) opens up to a certain critical value ($w_c$), stresses continue to transfer across the newly-formed part of the crack faces, since the aggregate pieces "bridge" the crack. Once the crack has opened beyond $w_c$, the newly-formed crack faces become traction-free. The energy required to open the new part of the crack faces from its initial intact state to the current traction-free state is $G_{CI}$. Thus, $G_{CI}$ of a concrete depends on the magnitudes of both $f_t$ and $w_c$. Typically, $f_t < 5$ N/mm$^2$ and $w_c < 0.2$ mm [13] which results in a relatively low $G_{CI}$ (usually, $G_{CI} < 0.15$ N/mm).

### 3.2. Mechanism and fracture energy of Mode II fracture

To propagate a crack in shear, the two crack surfaces need to displace relative to each other over the whole length of the fracture plane (Fig. 4b). Therefore, large crack plane separations, of the same order of magnitude as the size of the aggregate (typically, greater than 10 mm in size), are required to propagate a Mode II crack in concrete. A crack needs to follow a tortuous path and to propagate against high aggregate interlock resistances in comparison to the much lower $G_{CI}$, where crack plane separations of less than 0.2 mm triggers a crack. There is a large scatter in the $G_{CII}$ values reported in the literature (may be attributed to the different fracture areas experienced in different test specimens) and typically the values are about 20 times higher than $G_{CI}$ [14].

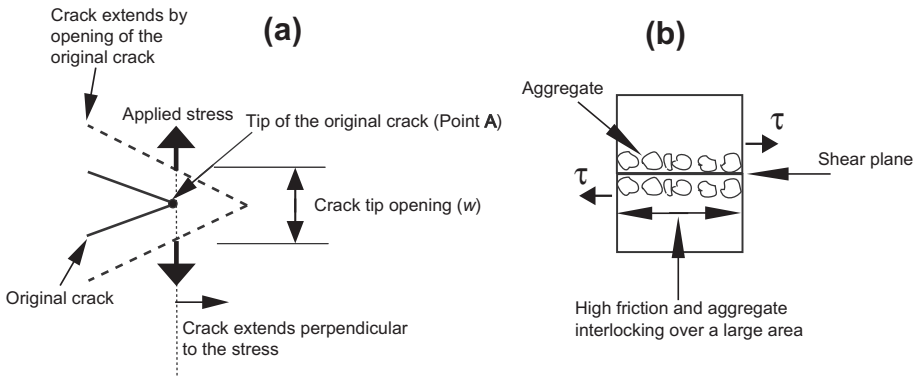


**Fig. 4.** (a) Mode I crack propagation. (b) High fracture resistance against a shear crack.

### 3.3. Local Mode I crack extension under mixed-mode loading

Because of the relatively high shear fracture resistance of concrete, it has been widely assumed that a crack under mixed-mode loadings propagates by opening of the crack tip, although the direction of propagation depends on the mode mixity [14]. It has been further assumed that a crack starts to open when the maximum principal tensile stress (MPTS) at the crack tip reaches $f_t$, and the instantaneous propagation will be in the direction perpendicular to that of the MPTS [14]. Thus, it is appropriate to assume that the crack opening will be associated with the same fracture energy as that under pure Mode I. This assumption has been widely validated in the literature [14]; the test results for the fracture paths matched well with that obtained from FE simulations based on the MPTS failure criterion with $G_{CI}$ as the governing parameter. It should be noted that these FE analyses would not have been affected by non-linear material behaviour because of the very low working strains, and also the fact that the test specimens should have been free from cracks other than the one where propagation was studied.

## 4. Mode I fracture energy of the concrete–FRP interface

It has been assumed here that, irrespective of the mode mixity, a crack in concrete will grow locally by opening in the direction perpendicular to MPTS. In this way, an interface of a strengthened beam, which is primarily carrying shear, actually fails in tension. In PE debonding, the $F_p$ acts eccentrically to the tip of the shear crack that triggers debonding, causing a moment that causes dominant tension in the crack tip, and hence the crack propagates by opening of the crack tip (Fig. 3a). During IC debonding, there is no moment induced by the FRP, which remains attached to the concrete at both ends of the unbonded zone (Fig. 3b). However, this attachment means that only infinitesimal sliding can take place and the large fracture energy associated with Mode II fracture cannot be developed. However, because the FRP is so thin and less stiff, it is relatively easy for it to move slightly away from the concrete surface, thus mobilising the much lower Mode I fracture energy.

### 4.1. Bond-slip models

Single/double-shear-lap experiments (Fig. 5a) have commonly been used [15] in the literature to determine the parameters for the analysis of FRP debonding. The specimens failed due to shear fractures that occurred within the concrete substrate, adjacent to the concrete–FRP interface. The maximum shear stress that can be resisted by the interface and the fracture energy were usually determined using the bond–slip relationships measured in the tests. The present authors assert that these tests do not provide meaningful fracture parameters that can be used in the analysis because the tests provide an estimate of Mode II fracture energy whereas a Mode I fracture triggers debonding. Fracture energy values derived from the tests (i.e. $G_{CII}$) were significantly higher than that against FRP debonding, and they also depend on the area of the fracture plane that has been formed in the experiment. For instance, tests with different widths of FRPs on identical concrete blocks resulted in different fracture energies [15]. A few recent studies on the analysis of FRP debonding [9], have used the bond-slip results derived from shear-lap tests, in smeared-crack FE models to analyse FRP debonding. The selection of Mode II fracture parameters in the models, however, does not represent the actual mechanism of FRP debonding.

Some recent research studies have experimentally investigated the Mode I fracture energy in the vicinity of concrete–FRP interface [16], although the tests were not aimed modelling FRP debonding as a Mode I fracture of concrete. Qiao and Xu [16] used a modified three-point bend specimen, where the specimen was made by joining two halves of the beam, one having an epoxy bonded FRP and the other an adhesive layer on the joining surfaces (Fig. 5b). A Mode I fracture was observed, within the concrete substrate at one side of the beam, but close to the interface. The fracture energy calculated from this study [16] is of similar magnitude to that of pure concrete (0.1–0.15 N/mm). Thus, the result illustrates that if the failure takes place within the concrete, the presence of nearby FRP does not affect fracture energy ($G_{CI}$).

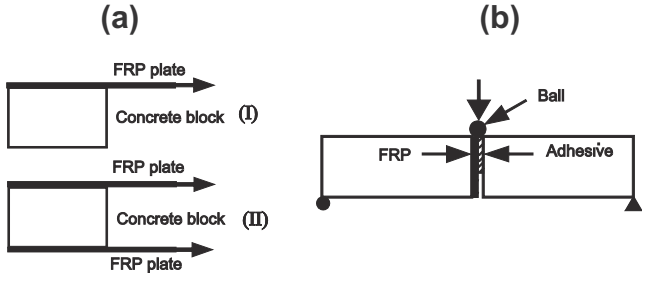


**Fig. 5.** (a) (I) – single (II) – double shear lap specimens. (b) A three-point bend specimen.

## 5. Invariance of the fracture energy during FRP debonding

When a fracture develops in a large block of concrete, it is possible for the FPZ to fully develop. The energy required to extend the crack can thus be expected to vary as the crack gets longer; that variation is referred to in fracture mechanics literature as *R*-curve. Although *R*-curve analyses of some non-linear materials, such as steel and FRP composites, are now well established, no accepted data exists for concrete. Although a few studies, such as the equivalent-LEFM-based model of Shah and Ouyang [17] have been reported, no conclusions were drawn. During a test, it is difficult to identify the FPZ when the crack has just formed, while the existence of a large FPZ (typically over 300 mm long with a width of the several times the aggregate size) means the results are influenced by the geometry of the test specimens. Typically, cover for the tension steel in the beams tested in laboratories is less that about ~30 mm and thus debonding cracks will be mostly with the size of this order. The effect is that the full FPZ cannot be developed ahead of debonding crack tip. Therefore, it is expected that full FPZ will not be developed during debonding and that means the *R*-curve does not reach a plateau during debonding. Despite considerable research during the 1980s, there has been very little work recently on the *R*-curve analysis of concrete. No advances over earlier understanding have been observed, even in the limited recent studies [17]. Even for cement paste, which has a much simpler microstructure, there is no consistent data.

Fig. 6 shows a crack forming in the cover zone of a beam; two positions are shown, one before and one after the interface crack has extended. Both the steel and the FRP are bonded to the concrete ahead of the crack, so the strain in the concrete is limited. The effect is that the FPZ ahead of the crack tip is of limited extent, and it cannot be influenced by the crack length, because it is not possible for any deformation of the FRP (the concrete being sensibly rigid) to change the state ahead of the crack tip. Thus, the FPZ in States 1 and 2 are of the same size, and hence the fracture energies must be independent of the crack length.

The corollary of this argument is that the fracture energy to be used in a debonding analysis should be the value obtained from small-scale test specimens, or from the initial stages of tests on larger specimens when the FPZ has not fully developed. This is consistent with earlier analyses of FRP debonding [3] that have shown that cracks of about 20–30 mm and 2–5 mm long cause PE and IC debonding respectively (note: length of the FPZ ~ 300 mm).

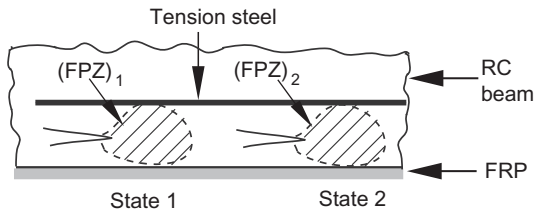


**Fig. 6.** Crack before and after extension.

## 6. Determination of the Mode I fracture energy of concrete

Knowledge of the stress vs. crack-opening ($\sigma$–$w$) relationships in the FPZ, during a unit extension of a Mode I crack, is required to determine Mode I fracture energy ($G_{CI}$). However, this analysis is not trivial since the $\sigma$–$w$ relationships of concrete depend on many microstructural features which are unknowable. No accepted method is reported in the literature for this analysis, and therefore, it is more accurate to determine $G_{CI}$ of a given concrete using experiments.

### 6.1. Experimental evaluation of $G_{CI}$

Standard methods [19] based on energy balance during the experiments of notched–beam specimens, together with appropriate correction factors, which are mostly empirically/semi-empirically derived, to take account of the effects due to small test specimens, are now well established to determine $G_{CI}$. It should, however, be appreciated that the incorporation of correction factors in the experimental results means that a fully-experimental procedure cannot be followed. As confirmed by recent studies [18], these experiments can be used to obtain reliable estimates for $G_{CI}$. Note that inaccurate $G_{CI}$ evaluations have been made, and are still being made, based on an empirical formula quoted in the CEB–FIP model code [13], which is simple to use, because it is based on the compressive strength ($f_c'$) and the maximum size of the aggregates ($d_a$) of the concrete. However, this formula was based on an earlier RILEM report [20] that recommends the direct estimation of $G_{CI}$ from the results of beam specimens without taking account of the size effect of concrete; thus, the method underestimates $G_{CI}$ in most cases.

### 6.2. Simplified approximate models for $G_{CI}$

Although it is possible to obtain reliable estimates for $G_{CI}$ from tests, the experimental investigations are not trivial and are often associated with several practical and conceptual difficulties. A stiff testing machine is needed to allow stable

fractures in concrete. Simplified models, albeit approximate, which are usually presented in terms of more readily known properties of concrete such as $f_c'$ and $d_a$ , are useful to determine $G_{Cl}$ .

### 6.3. The cohesive crack model

The cohesive crack model [21], which models the development of the FPZ by the stress vs. crack-opening relationship at the tip of a crack, is widely believed to be the best performing fracture model for concrete and is widely used in the fracture analysis of concrete. The model is also very useful in experimental studies since only the characteristics at the original crack tip, whose geometric location is precisely known, need to be studied.

A crack is assumed to open when stress at the tip of the FPZ ($\sigma_{tip}$) reaches $f_t$. Thus, at the tip of the fracture process zone (FPZ) (Point A in Fig. 7), a zero crack opening is associated with a $\sigma_{tip}$ of $f_t$. The widening of this tip of the FPZ ($w_{tip}$) causes the crack to propagate. However, the aggregate pieces bridge the FPZ and hence there will only be a gradual decrease in $\sigma_{tip}$ to zero as $w_{tip}$ grows to a critical value ($w_{tip\_c}$) where there is no stress transfer between the crack surfaces in the FPZ. The $\sigma_{tip}$–$w_{tip}$ relation is referred to as the tension-softening response, and it is assumed that the part of the crack opening where $w_{tip} < w_{tip\_c}$ characterises the development of the FPZ. The area under the $\sigma_{tip}$–$w_{tip}$ curve (Fig. 7) – i.e. work done against cohesive forces present in the FPZ (Eq. (2)) – represents $G_{Cl}$. The model thus provides an alternative way to estimate $G_{Cl}$, avoiding the need for knowledge of the stress–crack opening relations in the entire FPZ. This has the advantage that the location of the tip of the FPZ is usually known and hence the opening characteristics can be experimentally determined to an acceptable accuracy whereas reliable data cannot be known to analyse the entire FPZ.

$$\int_0^{w_{tip\_c}} \sigma_{tip} dw_{tip} = G_{Cl} \tag{2}$$

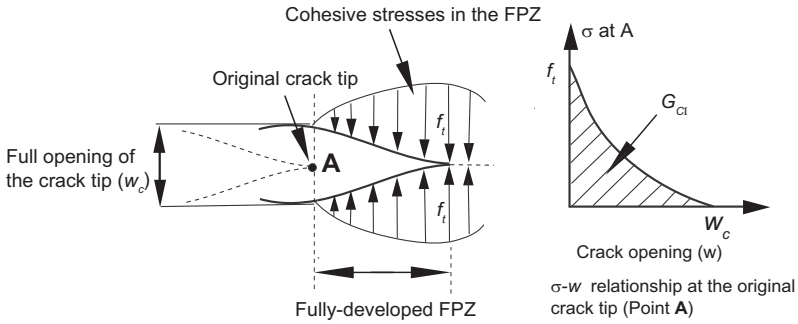


**Fig. 7.** Cohesive crack model (Hillerborg et al. [21]).

### 6.4. Tensile strength and the tension-softening response

The tensile strength ($f_t$) and the tension-softening response are both required to determine $G_{Cl}$.

#### 6.4.1. Tensile strength

The $f_t$ of a concrete can be influenced by the heterogeneity of the mix and also the type of stress field that causes the failure. However, it is generally assumed to have a known relation to the $f_c'$ of the mix; the EuroCode 2 [22] recommendation is used in the present work (Eq. (3)).

$$f_t = 0.30(f_c')^{2/3} \text{ (in N/mm}^2 \text{ units)} \tag{3}$$

#### 6.4.2. Determination of the tension-softening response

The softening response of concrete usually determined based on uniaxial tensile tests which carried out using stiff testing machines [23]. However, the location of the fracture is not known *a priori*, so study of the FPZ prior to the growth of microcracks is very difficult. A notched specimen helps to locate the FPZ, but the notch introduces a stress concentration. During a test it was generally assumed a uniform stress distribution across the specimen, but once a crack has initiated a significant stress gradient will develop near the crack. Despite it is difficult to obtain precise results for the exact $\sigma$–$w$ relationships, the tests are capable of providing the approximate shape of the softening curve. This can then be adjusted until the area under the curve equals the independently determined more reliable estimate of $G_{Cl}$. This allows the correlation of the softening curve with more readily-known properties of concrete such as $f_c'$ and $d_a$. The models can then be used for the estimation of $G_{Cl}$ of other concretes.

### 6.5. Simplified tension-softening models

A rapid development of microcracks followed by stable widening of a critical macrocrack was observed in the tests [24]. Thus, the shape of the softening curve has been approximated by using bilinear [24] and polynomial [25] models with $f_t$ and $w_{tip\_c}$ as the key parameters (Fig. 8).

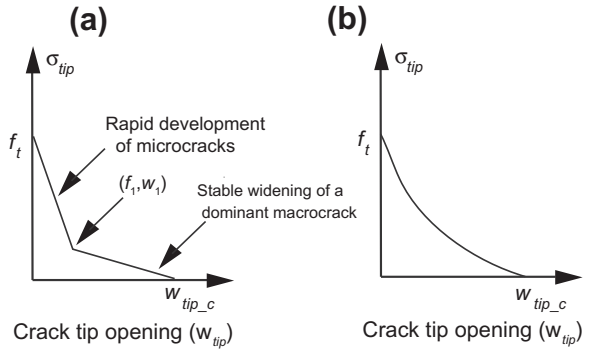


**Fig. 8.** Simplified tension-softening models (a) bilinear and (b) polynomial.

#### 6.5.1. Bilinear models

In bilinear models, the coordinates of the kinking point ($f_1$, $w_1$), and $w_{tip\_c}$ are required to determine $G_{Cl}$ (Fig. 8a). It has been reported that $f_1$ is about 1/3 of $f_t$ [24], and a range of values between 0.03 and 0.04 mm were quoted for $w_1$ [23,24]; these values are assumed in the present study. The stress transfers between the crack surfaces, and hence, $w_{tip\_c}$, depend upon $d_a$ of the mix. The CEB–FIP model code [13] recommends typical $w_{tip\_c}$ values of 0.12, 0.15 and 0.25 mm for concretes with crushed aggregate of 8, 16 and 32 mm respectively. In the present study, these values are assumed with appropriate interpolations to determine $w_{tip\_c}$ of concretes with other sizes of aggregate.

#### 6.5.2. Polynomial models

The power relation developed by Reinhardt [25] is the most widely quoted polynomial model in the studies.

$$\sigma = f_t\lfloor 1 - (w/w_c)^n \rfloor \tag{4}$$

where $n$ is the fitting parameter which he found to be between 0.2 and 0.4 for normal concrete [25].

The more recent studies of tension-softening of concrete [26] were still based on previously-described simplified models, although newer test set-ups were used together with improved crack-detection techniques such as digital image correlations. However, no improvements in understanding over the earlier simplified models have been reported.

#### 6.5.3. Effects of the shape and the surface texture of aggregates

In concretes with rounded aggregate (e.g. river gravels), the macrocracks may coalesce by growing around the aggregate pieces. However, when rough/angular aggregate (e.g. crushed aggregate) are used, the macrocracks may follow the shortest path by growing through the aggregate pieces because of the high frictional resistances along tortuous crack paths. As a result, crushed aggregates give higher $G_{Cl}$. The simplified tension-softening models discussed above were based on results of concretes with crushed aggregates, and therefore, the models do not take account of the effects due to the shape and the surface texture of the aggregate. The empirical model of Bažant and Becq-Giraudon [27], based on a large database of test results, takes account of these effects to predict $G_{Cl}$. They quote (Eq. (5)):

$$G_{Cl} = 2.5\alpha_0(f'_c/0.051)^{0.46}(1 + d_{a\_max}/11.27)^{0.22}(W/C)^{-0.30} \ (\text{N, mm units}) \tag{5}$$

where $\alpha_0 = 1$ and 1.44 for rounded and crushed aggregates respectively, and $W/C$ is the water/cement ratio by weight of the mix.

**Table 1**
Estimation of $G_{Cl}$ of the assumed concrete mix.

| Reference | Model | $G_{Cl}$ (N/mm) |
|---|---|---|
| Gustafsson and Hillerborg [28] | Bilinear softening | 0.140 |
| Reinhardt [25] | Power relation | 0.083–0.142 |
| Guinea et al. [24] | Bilinear softening | 0.145 |
| Bažant and Becq-Giraudon [27] | Empirical | 0.112 ± 0.034 |
| CEB–FIP model code [13] | Empirical | 0.0825 ± 0.025 |

### 6.6. Estimation of $G_{Cl}$: an example

Table 1 shows the estimates for $G_{Cl}$ for a concrete mix with $d_a$ of 20 mm (crushed aggregate) and W/C of 0.5 according to the simplified softening models and empirical models discussed above. The polynomial model gives a range of values to be expected from tests but does not give a method for predicting the exact value without doing tests. As shown in Table 1, the predictions from all methods but the CEB–FIB model code expression [13] match well. As expected, the CEB–FIB expression underestimates $G_{Cl}$. The results suggests a value of 0.15 N/mm for $G_{Cl}$ of this concrete, which agrees with experimentally noted $G_{Cl}$ for similar strength concretes with crushed aggregates of 20 mm [18]. It has been shown that the incorporation of $G_{Cl}$ determined this way in the debonding analysis gives predictions that match the test results reported in the literature [3]. The $G_{Cl}$ values used in that study were determined as below.

## 7. Use of $G_{Cl}$ in the analyses of FRP debonding

The global-energy-balance FRP debonding analysis was applied to several sets of beam tests reported in the literature [3]. The $G_{Cl}$ of the concretes used were not measured, so it is necessary to decide on values that can be used in the analysis. The $f'_c$ of the concretes used in the beams being tested were in the range 30–55 N/mm$^2$; crushed aggregates of 20 and 10 mm and 10 mm rounded aggregates were used in the mixes [3]. Since the $f'_c$ of the beams did not vary significantly, it was assumed that variations in $G_{Cl}$ of these concretes mainly depend on the aggregate properties. Table 2 shows the estimates for $G_{Cl}$ of the beams under consideration, calculated from data quoted by the experimenters, according to the simplified models and the empirical model discussed above. Since the softening models can only be used to estimate $G_{Cl}$ of concretes with crushed aggregates, the $G_{Cl}$ of the mixes with rounded aggregate were estimated using the empirical model only. When using the bilinear models, the coordinates of the kinking point ($f_1$, $w_1$ in Fig. 8a) were assumed to be $0.33f_t$ [24] and 0.03 mm [25] respectively, for all concretes. The values of $f_t$ were obtained from Eq. (3). The values for the $w_{tip\_c}$ of concretes with 10 and 20 mm crushed aggregates were assumed to be 0.130 and 0.175 mm respectively, based on the typical values recommended in the CEB–FIP model code [13].

Based on the values quoted in Table 2, the $G_{Cl}$ of mixes with crushed aggregates of 20 and 10 mm; and 10 mm rounded aggregates were assumed to be 0.15, 0.10 and 0.07 N/mm respectively. These values agree with experimentally-obtained $G_{Cl}$ values for concretes with similar properties [18]. The measured $G_{Cl}$ values were often associated with a scatter of about 10%, so to illustrate the significance of this variability, results for a ±10% variation in $G_{Cl}$ was considered in the debonding analysis.

**Table 2**
Estimation of $G_{Cl}$ of studied concrete beams.

| Aggregate type | Reference | $G_{Cl}$ (N/mm) | | | | |
|---|---|---|---|---|---|---|
| | | Estimates from the models | | | | |
| | | Bilinear models | | Polynomial model | Empirical model | Assumed $G_{Cl}$ for debonding analysis |
| | | Gustafsson and Hillerborg [28] | Guinea et al. [24] | Reinhardt [25] | Bažant and Becq-Giraudon [27] | |
| 20 mm Crushed | Fanning and Kelly [29] | 0.18 | 0.17 | 0.12–0.21 | 0.13 | |
| | Nguyen et al. [30] | 0.15 | 0.14 | 0.10–0.18 | 0.12 | 0.15 |
| | Garden et al. (Beam $1_{U,4.5}$) [31] | 0.15 | 0.14 | 0.10–0.18 | 0.12 | |
| 10 mm Crushed | Jones et al. [32] | 0.12 | 0.10 | 0.08–0.11 | 0.10 | |
| | Ross et al. [33] | 0.13 | 0.11 | 0.09–0.13 | 0.11 | 0.10 |
| | Garden et al. (Beam $3_{U,1.0}$) [31] | 0.12 | 0.10 | 0.08–0.11 | 0.10 | |
| 10 mm Rounded | Arduini et al. [34] | N/A | N/A | N/A | 0.068 | |
| | Quantrill et al. [35] | N/A | N/A | N/A | 0.073 | 0.07 |

### 7.1. Results of debonding analyses

The authors have previously developed a fracture mechanics model to analyse FRP debonding; this model requires knowledge of the fracture energy of concrete to predict the load at which the FRP debonds from the concrete beams. It has been shown that the incorporation of the fracture energy, determined using the methods described in the current paper, in the FRP debonding model predicted results that match the experimental data. In this main study, a large database of beam specimens, including a variety of material and geometric properties, and also covering beams that failed in all possible modes of FRP debonding, was investigated. Due to the space limitation only the FRP debonding analysis of a single example for each of plate-end (PE) and intermediate-crack-induced (IC) debonding are shown below. The readers are referred to the previous large study [3] for details of the complete database of test results used to validate the FRP debonding model.

All the beams analysed in the study [3] were tested as simply-supported beams under four-point bending with equal shear spans. For each chosen example, the energy release rate ($G$) corresponding to an assumed debonding crack at the reported failure load ($P_f$) is compared with the Mode I fracture energy of concrete ($G_{Cl}$), determined according to the methods described in the current paper. It should be noted that to take account of the uncertainty of all the parameters and to illustrate the significance of the variability, the results for a ±10% variation in $P_f$ and a ±10% variation in $G_{Cl}$ are considered.

*7.1.1. Example: plate-end debonding*

When the FRP is curtailed at a considerable distance away from the beam support, debonding is likely to initiate due to the formation of a critical shear crack near to the FRP end. Further extension of this crack forms an interface crack, so the effective plate end location ($L_{0\_e}$), just prior to the initiation of rapid propagation of debonding, is now placed slightly away from the actual plate end ($L_0$) (Fig. 9). It was assumed that the original shear crack propagates along a direction at about 45° to the interface (the actual direction may be slightly varied from this, but it should not have a significant effect on the results), up to the level of tension-steel bars in the beam. Thus, it was contended that $L_{0\_e}$ should be located between $L_0$ and a further cover distance ($c$) into the beam (Fig. 9). Energy release rate ($G$) associated with $L_{0\_e}$ values in the range $L_0$–$2c$ and $L_0$+$2c$ were calculated and compared with $G_{Cl}$ (including a range with ±10% variation) to decide whether debonding is possible at the observed failure load ($P_f$).

Fig. 10 shows the variation in $G$ vs. $L_{0\_e}$ for beam pair F9 and F10 selected from the study of Fanning and Kelly [29] ($L_0$ = 500 mm and $c$ = 30 mm). The $G_{Cl}$ of the concrete with 20 mm crushed aggregate was determined to be 0.15 N/mm (Table 2). The figure shows that taking $L_{0\_e}$ to be 10 mm higher than the actual $L_0$ (i.e. $L_0 < L_{0\_e} < L_0 + c$), the failure load predicted from the model compares well with the $P_f$ observed in the experiment. The figure also shows that, at the observed $P_f$ any $L_{0\_e}$ shorter than the actual $L_0$ could not cause PE debonding, since an interface crack of a positive magnitude is required

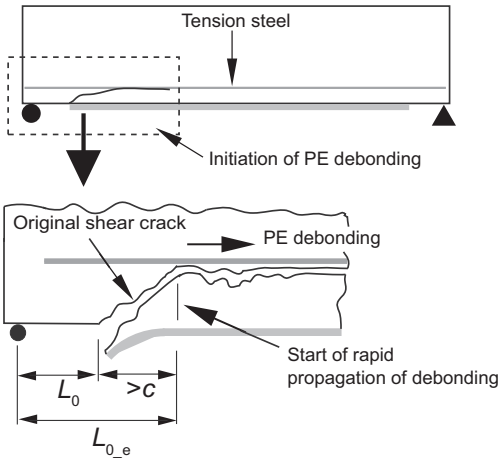


**Fig. 9.** Location of the effective plate end.

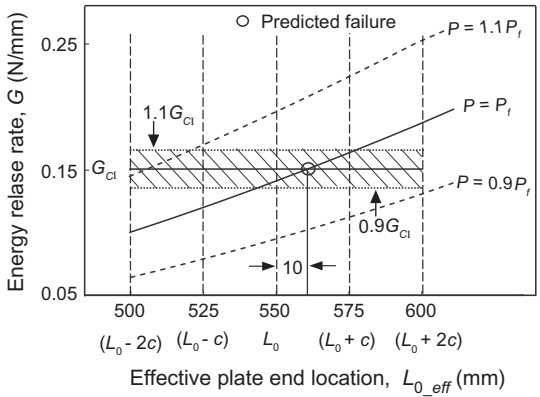


**Fig. 10.** $G$ vs. $L_{0\_eff}$ plots for beam set F9 and F10 (Fanning and Kelly [29]).

to trigger failure. Fig. 10 also shows that loads 10% higher or lower than $P_f$ are too strong or too weak respectively to cause failure within the range between $L_0$ and $L_0 + c$. Thus, the results of the present analyses match with the observed $P_f$ and failure mode.

*7.1.2. Example: intermediate-crack-induced debonding*

Earlier analyses by the authors [3] have shown that, in four-point bending beams, interface cracks formed due to widening of flexural cracks located at about a half beam depth ($h$) away from the loading point cause IC debonding (Fig. 11). Analyses of IC debonding observed in a set of beams (Group 1) reported in the study of Ross et al. [33] are discussed below.

Possible propagation of interface cracks that are assumed to initiate at the critical location ($x_c$) of the beam span (i.e. ½ $h$ away from the loading point) and, a further ½ $h$ and $h$ towards the nearest beam end were investigated. A concrete with 10 mm crushed aggregate was used in the beams, so $G_{CI}$ was determined to be 0.10 N/mm (Table 2). The solid line in Fig. 12a shows the variation in $G_R$ vs. $l_d$ (crack length) for an interface crack that initiates at $x_c$, at the observed $P_f$. The figure

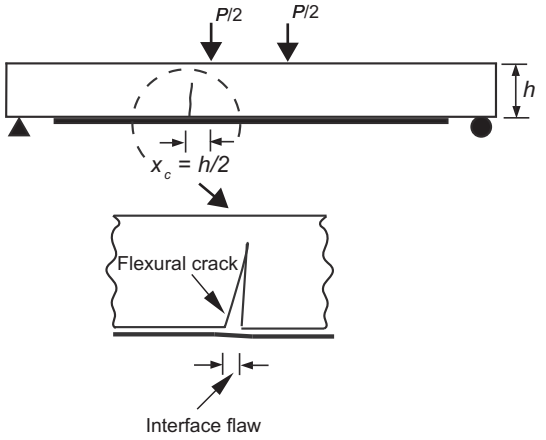


**Fig. 11.** Initiation of IC debonding by widening of flexural cracks.

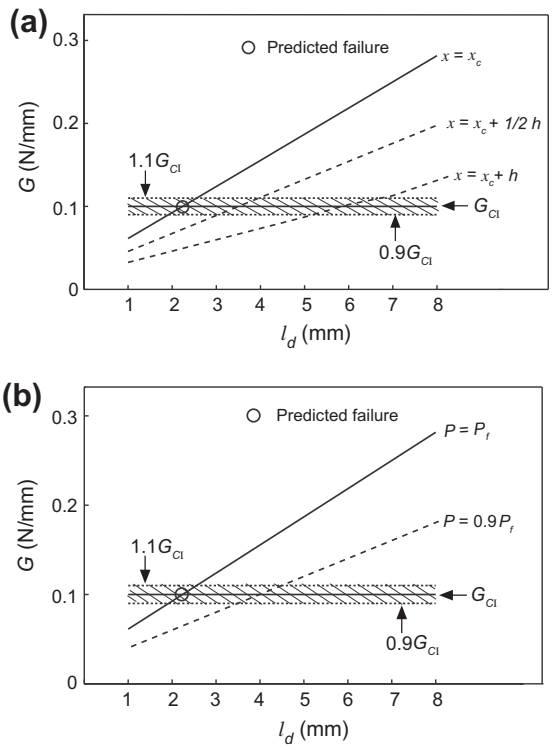


**Fig. 12.** $G$ vs. $l_d$ plot for Group 1 beam (Ross et al. [33]) for fractures starting at (a) different locations and (b) 90% of the failure load.

shows that $l_d$ of 2 mm would cause failure here; it has been observed that widening of a critical flexural crack in the high moment zone forms interface cracks of this magnitude [31]. The dashed lines in Fig. 12a show that, if the debonding initiated at ½ $h$ or $h$ away towards the nearest beam end, much longer cracks of lengths 3.5 mm and 6 mm respectively, would be required to cause debonding at $P_f$; these are less likely to occur. The conditions needed for debonding to initiate at $x_c$ at 90% of $P_f$ is also investigated in Fig. 12b. The figure shows that a critical crack of length about twice that required at $P_f$ would be required to cause failure here so again is less likely.

## 8. Conclusions

- The paper has shown that the FRP force, acts with an eccentricity with respect to the tip of the crack that triggers plate-end debonding, causes a dominant tension in the crack tip, and hence the crack starts to propagate by opening.
- In intermediate-crack-induced debonding, the FRP cannot slide parallel to the concrete because it is fixed at both ends of the unbonded zone, but it can move away from the surface, thereby causing Mode I crack initiation.
- Even though the interface of a strengthened beam is primarily carrying shear, it actually fails in tension. Thus, FRP debonding propagates locally as a Mode I fracture in concrete.
- Debonding occurs in a narrow zone of concrete, between the FRP and the internal steel bars of the beam, and therefore, a conventional fracture analysis of the fracture process zone, which is typically over 300 mm long, cannot be performed.
- It is appropriate to assume that the fracture energy to be used in a debonding analysis should be the value obtained from small-scale test specimens.
- Appropriate models to determine the Mode I fracture energy of concrete, to an accuracy that can be used in the analysis of FRP debonding, have been presented. A single example for the debonding analysis of each of plate-end and intermediate-crack-induced debonding has shown in the paper. Details of the debonding analysis of a large database of test beams were presented elsewhere.
- The incorporation of the Mode I fracture energy of concrete in the FRP debonding analyses, gives predictions that match the experimental results reported in the literature.

## References

[1] Achintha M, Burgoyne CJ. Moment-curvature and strain energy of beams with external FRP reinforcement. ACI Struct J 2009;106(1):20–9.
[2] Achintha M, Burgoyne CJ. Fracture mechanics of plate debonding. J Compos Constr 2008;12(4):396–404.
[3] Achintha M, Burgoyne CJ. Fracture mechanics of plate debonding: validation against experiments. Constr Build Mater 2011;25(6):2961–71.
[4] Büyüköztürk O, Günes O, Karaca E. Progress on understanding debonding problems in reinforced concrete and steel members strengthened using FRP composites. Constr Build Mater 2004;18(1):9–19.
[5] Hutchinson JW, Suo Z. Mixed mode cracking in layered materials. Adv Appl Mech 1992;29:63–191.
[6] Karihaloo BL. Fracture mechanics and structural concrete. England: Addison Wesley Longman Limited; 1995.
[7] Kotsovs MD, Pavlovic A. Structural concrete. London: Thomas Telford Publications; 1995.
[8] Achintha M. Fracture analysis of debonding mechanism for FRP plates. PhD thesis. UK: University of Cambridge; 2009.
[9] Wang J, Zhang C. Nonlinear fracture mechanics of flexural-shear crack induced debonding of FRP strengthened concrete beams. Int J Solids Struct 2008;45(2):2916–36.
[10] Oehlers DJ, Ali MSM, Haskett M, Lucas W, Muhamad R, Visintin P. FRP-reinforced concrete beams: unified approach based on IC theory. J Compos Constr 2011;15(3):293–303.
[11] Achintha M, Burgoyne C. Prediction of FRP debonding using the global-energy-balance approach. Mag Concr Res 2012;64(11):1033–44.
[12] Branson DE. Design procedures for computing deflections. ACI J 1968;65(9):730–5.
[13] Comite Euro-International du Beton-Federation Internationale de la Precontrainte. CEB–FIP Model Code. Lausanne: Switzerland; 1991.
[14] Gálvez JC, Elices M, Guinea GV, Planas J. Mixed mode fracture of concrete under proportional and nonproportional loading. Int J Fract 1998;94(3):267–84.
[15] Subramaniam KV, Carloni C, Nobile L. Width effect in the interface fracture during debonding of FRP from concrete. Engng Fract Mech 2007;74(4):578–94.
[16] Qiao P, Xu Y. Evaluation of fracture energy of composite–concrete bonded interfaces using three-point bend tests. J Compos Constr 2004;8(4):352–9.
[17] Shah SP, Ouyang C. Fracture mechanics for failure of concrete. Annu Rev Mater Sci 1994;24:293–320.
[18] Karihaloo BL, Abdalla HM, Imjai T. A simple method for determining the true fracture energies of concrete. Mag Concr Res 2003;55(5):471–81.
[19] Shah SP, Carpinteri A, editors. Fracture mechanics test methods for concrete – RILEM Report 5. London: Chapman & Hall Publisher; 1991.
[20] RILEM Committee 50-FMC. Determination of the fracture energy of mortar and concrete by means of the three-point bend tests on notched beams. Mater Struct 1985;18(4): 287–90.
[21] Hillerborg A, Modéer M, Petersson PE. Analysis of crack formation and crack growth in concrete by means of fracture mechanics and finite elements. Cem Concr Res 1976;6(6):773–82.
[22] British Standards Institution. Eurocode 2: Design of concrete structures. Part 1-1: General rules and rules for buildings. London; 2004.
[23] Raiss ME. Observation of the development of fracture process zone in concrete under tension. PhD thesis; London: Imperial College; 1986.
[24] Guinea GV, Planas J, Elices M. A general bilinear fit for the softening curve of concrete. Mater Struct 1994;27(2):99–105.
[25] Reinhardt HW. Crack softening zone in plain concrete under static loading. Cem Concr Res 1985;15(1):42–52.
[26] Barr B, Lee MK. Modeling the strain-softening behaviour of plain concrete using a double-exponential model. Mag Concr Res 2003;55(4):343–53.
[27] Bažant ZP, Becq-Giraudon E. Statistical prediction of fracture parameters of concrete and implications for choice of testing standard. Cem Concr Res 2001;32(4):529–56.
[28] Gustafsson PJ, Hillerborg A. Improvements in concrete design achieved through the application of fracture mechanics. In: Shah SP, editor. Application of fracture mechanics to cementitious composites. Dordrecht, The Netherlands; 1985. p. 639–80.
[29] Fanning PJ, Kelly O. Ultimate response of RC beams strengthened with CFRP plates. J Compos Constr 2001;5(2):122–7.
[30] Nguyen DM, Chan TK, Cheong HK. Brittle failure and bond development length of CFRP–concrete beams. J Compos Constr 2001;5(1):12–7.
[31] Garden HN, Quantrill RJ, Hollaway LC, Thorne AM, Parke GAR. An experimental study of the anchorage length of carbon fibre composite plates used strengthened reinforced concrete beams. Constr Build Mater 1998;12(4):203–19.

[32] Jones R, Swamy RN, Charif A. Plate separation and anchorage of RC beams strengthened by epoxy-bonded steel plates. The Struct Eng 1988;66(5):85–94.
[33] Ross CA, Jerome DM, Tedesco JW, Hughes ML. Strengthening of reinforced concrete beams with externally bonded composite laminates. ACI Struct J 1999;96(2):212–20.
[34] Arduini M, Di Tommaso A, Nanni A. Brittle failure in FRP plate and sheet bonded beams. ACI Struct J 1997;94(4):363–70.
[35] Quantrill RJ, Hollaway LC, Thorne AM. Experimental and analytical investigation of FRP strengthened beam response: Part I. Mag Concr Res 1996;48(4):331–42.